FIFTH INTERNATIONAL CONGRESS ON SOUND AND VIBRATION
DECEMBER 15-18, 1997
ADELAIDE, SOUTH AUSTRALIA

The Low Frequency Acoustic Loading Vibration Response Analysis of Structures

Keiko Yoshida

Mitsubishi Electric Corporation
Advanced Technology R&D Center

The purpose of this study is to analize the vibration response of spacecraft structures, especially lightweight rigid panels, such as solar array paddles and antennas, when excited by a low frequency acoustic noise field. First, the direct loading pressure on a structure in a random sound field is derived and a response calculation method using FEM is proposed. Second, the derivation of the direct loading pressure to the structure is experimentally verified in the steady-state sound pressure field, using a honeycomb panel whose edge was bolted to a stand. Finally, the experimental results of the acceleration responses of the panel in the random sound field are found to agree with the simulation results of the proposed calculation method. The simulation results of the usual frequency response method contain a high degree of error compared with the results of the new method. This method is applied to a practical antenna panel, and the results of the simulation agree with the acoustic test.

1. Introduction

Because the solar array paddles and antennas of spacecraft have become larger and lighter recently, the acoustic loading vibration of these structures has become a design problem: the natural frequency has become lower, and the amplitude has become bigger. The finite element method (FEM) is a powerful tool for analizing the vibration stress of the support of the structure.

Usually, statistical energy analysis (SEA)[1] or the power flow finite element method (PFFEM)[2] are used to solve acoustic loading vibration problems, because they are good at broad frequency band analysis, and they can deal with many modes within the frequency band.

However it is difficult to solve the details of the structural the stresses of each part, therefore, designers must estimate the acoustic loading vibration stress by FEM, calculating the force of each element according to the acoustic pressure and the element area, and by assuming that each force of the element is equally phased.

As the impedance of the structure becomes very small in the low frequency band and its value becomes to similar to the impedance of air, the interaction of sound and vibration will occurr and so the acoustic pressure near the structure will be different from one distant from the structure.[3] The spatial correlation of each part of the diffused sound pressure field has already been derived.[4–6] The vibration responses can be derived from this spatial distribution of the sound pressure using the power spectrum density (PSD). In this paper, first I derive the variation of the acoustic pressures near the structure in the low frequency band. Second, I show the acoustic loading vibration analysis by FEM considering the spatial correlation of the diffused sound pressure field, and compare the calculation and experiment. It is found that the proposed method is more accurate than the method usually used by designers.

2. Analysis

The analysis method was derived using these conditions,
(1) In the experiment, the echoic room was very large compared with the structure, and the acoustic field was diffused.
(2) The acoustic radiation efficiency was smaller than 1, and the sound pressure field except near the structure, did not change whether the structure was present or not.

In the diffused sound pressure field, the forces of each point satisfy a random process.[7] All the PSD of the sound pressure distant from the structure can be equally defined as $P_o^2(f)$, where f is the frequency. The real part of the cross PSD of the sound pressure $P_i(f)$ at point i and the sound pressure $P_j(f)$ at point j defined as $Re[P_i(f)P_j(f)^*]$ (the real part of the conjugate multi),[8] is

$$Re[P_i(f)P_j(f)^*] = P_o^2(f)sin(k|x|)/(k|x|), \tag{1}$$

where, k is the wave number of sound, and $|x|$ is the distance between point i and point j.

The particle velocity of the sound at the boundary between the structure and air is equal to the velocity of the structure, and, sound pressure near the structure arises corresponding to the particle velocity.[9] This phenomenon does not depend on whether the sound pressure field is diffused or not. By equalizing the pressure, the structural vibration velocity $v_k(f)$ can be expressed as,

$$v_k(f) = [P_k(f) - p_k(f)]/(\rho c), \tag{2}$$

where. $P_k(f)$ is the sound pressure with no structure at point k, $p_k(f)$ is the sound pressure near the structure at point k, ρ is the density of the air, and c is the speed of sound. By using modal analysis, when the number of finite elements is I, the number of structural vibration modes is R, and the sound pressure at point i is $p_i(f)$. Here, $v_k(f)$ is expressed as,

$$v_k(f) = \sum_{r=1}^{R} \frac{\phi_{rk}}{z_r(f)} \sum_{i=1}^{I} \phi_{ri} p_i(f) \Delta A_i, \tag{3}$$

$$z_r(f) = 2\pi m_r (f_r^2 - f^2 + j f_r f \eta_r)/f, \tag{4}$$

where, ϕ_{ri} is the rth mode of the structure at point i, ΔA_i is the equalized area at point i, $z_r(f)$ is the impedance of the structure, m_r is the modal mass, f_r is the natural frequency, and η_r is the loss factor of the rth mode of the structure. Equations (2) and (3) derive the relation of $p_i(f)$ and $P_i(f)$ like this,

$$\{p_i(f)\} = [X_{ij}]\{P_j(f)\}, \tag{5}$$

where, the element of $[X_{ij}]^{-1}$ is

$$\sum_{r=1}^{R} \frac{\phi_{ri}\phi_{rj}\rho c \Delta A_j}{z_r(f)} + \delta_{ij}, \tag{6}$$

where δ_{ij} is Kronecker's delta. From these equations it follows that the sound pressure level near the structure may be different from one distant from the structure, when the structural impedance becomes smaller than the acoustic impedance. By calculating equations (1) and (5), the real part of the cross PSD $Re[p_i(f)p_j(f)^*]$ by equation (5), is derived to,

$$Re[p_i(f)p_j(f)^*] = Re[\sum_{k=1}^{I}\sum_{l=1}^{I} X_{ik}(f)X_{jl}(f)^* P_o(f)^2 sin(k|x|)/(k|x|)]. \tag{7}$$

When the structure is loaded by the sound pressure expressed by equation (7), PSD $S_k(f)$ of the vibration at point k is,

$$S_k(f) = \sum_{r=1}^{R}\sum_{s=1}^{R} \frac{\phi_{rk}\phi_{sk}}{z_r(f) z_s^*(f)} \sum_{i=1}^{I} \phi_{ri} \{\sum_{j=1}^{I} \phi_{sj} Re[p_i(f)p_j(f)^*]\Delta A_j\}\Delta A_i. \tag{8}$$

For the algorithm of the numerical calculation, we first obtain the modal parameter from the FEM calculation or experiments, second calculate the impedance of the structure, and derive $[X_{ij}(f)]$ of equation (5), then derive the cross PSD of equation (7), and finally input it to equation (8). Before this algorithm was applied to the design calculation, the vibration was calculated under the condition that $P_o(f)$ was defined as $p_i(f)$, and the all sound wave phases of the between each point were the same.

3. Test panel and pre-examination

The test panel is a honeycomb panel, whose specification is shown in Table 1. It was fixed with 2 bolts to a heavy jig. Figure 1 shows the number of grids of the finite element analysis. To survey the modeling of the calculation, a modal test was applied to the test panel using a moving coil shaker. Figure 2 shows a 1st to 3rd mode comparison between the calculation and the test. The modal shapes and natural frequencies were

Table 1 The properties of the honeycomb panel (units: SI)

Parameter	Value
Mass per unit area	2.4 kg/m^2
Elastic Modulus of the face sheet	$7.06 \cdot 10^{10}$ N/m^2
Poisson's ratio of the face sheet	0.33
Area	1.0 m^2
Thickness of the face sheet	$0.3 \cdot 10^{-3}$ m
Thickness of the core	$24.4 \cdot 10^{-3}$ m
Fastening torque of bolts	300 kgm
Bolt diameter	M5

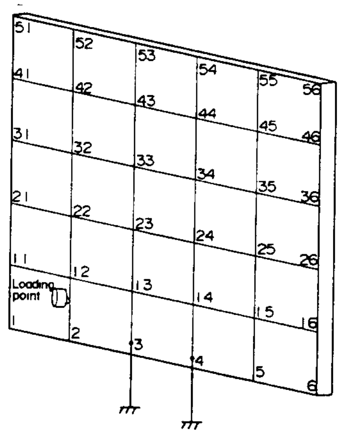

Fig. 1 Test panel

thus verified. For the proposed analysis I used the modal parameters from the calculation and the loss factors from the test.

Figure 3 shows the instrument circuit of the acoustic test, and Figure 4 shows the configuration in the echoic room. The lattice was made by strings (threads) in front of the panel, and it allows the SPL to be measured at the same point in each experiment with or without the panel. The acoustic tests used random white noise both for tests with a panel and without a panel. Figure 5 shows a comparison of the SPL between the two cases. There are 3 structural modes under 100 Hz, and a change of the SPL was found in the 3rd mode. No changes were found in the other modes. This was because the SPL below 20 Hz is very small for the frequency characteristic of the speakers and the small volume of the echoic room, and also the 2nd mode, which is unsymmetrical, is difficult to create with the acoustic pressure load.

To examine the change of the SPL with the structure and without it, at each point of the lattice of Figure 4 a sine wave sweep test was held from 65 Hz to 85 Hz at steps of 1 Hz intervals. The amplitudes and phases of SPL of each point of the sound field are different to each other. Therefore, to regulate the phase. Figure 6 shows the transfer function of the SPL of each point based on the SPL of a point 2m distant from the structure, which was investigated for points 3 and 25. It was found that the change of the SPL, with and without the

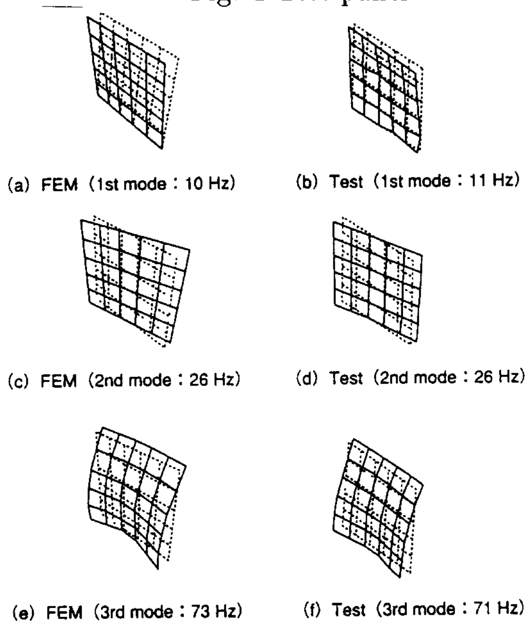

Fig. 2 The results of modal analysis

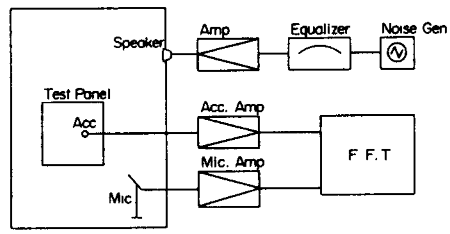

Fig. 3 The acoustic test circuit

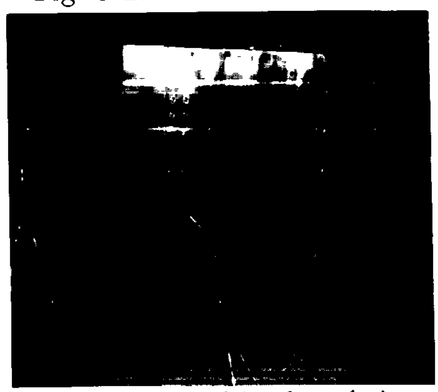
Fig. 4 The test panel in the echoic room

structure, depends on the frequency. By substituting the measurement value of the amplitude and the phase of $P_j(f)$ into equation (5), we can obtain the calculation value of $p_i(f)$, thus,

$$\alpha = 20log\frac{|p_i(f)|}{P_o(f)}. \tag{9}$$

Figure 7 shows a comparison of α according to the calculation value and measurement value of $p_i(f)$. Here α at 75 Hz at point 25 is about 20 dB, and the calculation result agrees with the experiment. This agreement shows the matrix of equation (5) is correct.

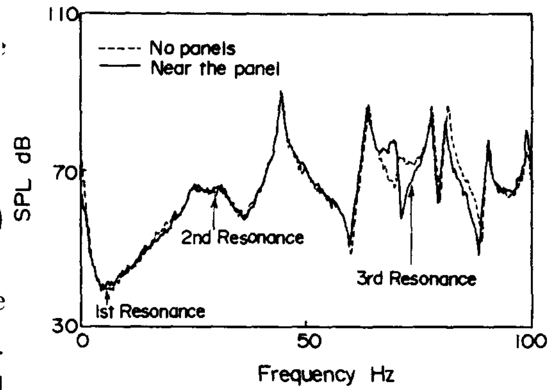

Fig. 5 Variance of SPL near the structure (point 44)

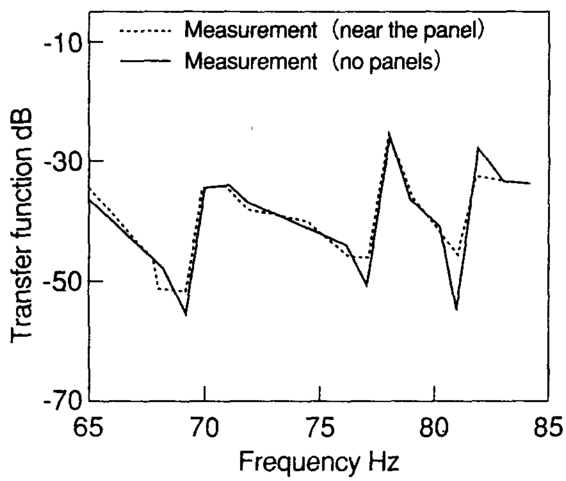

(a) point 3

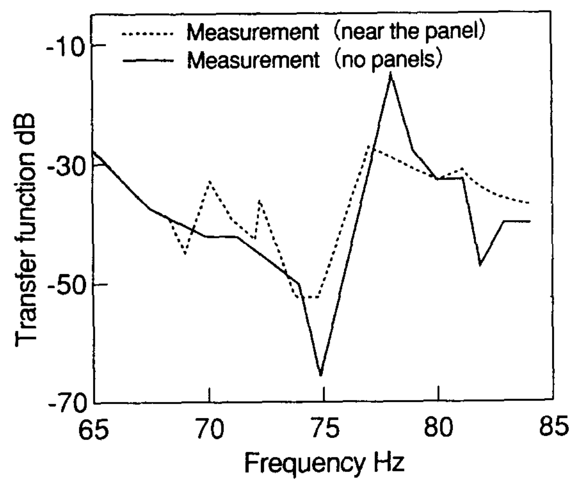

(b) point 25

Fig. 6 Comparison of the transfer function of the SPL near the structure

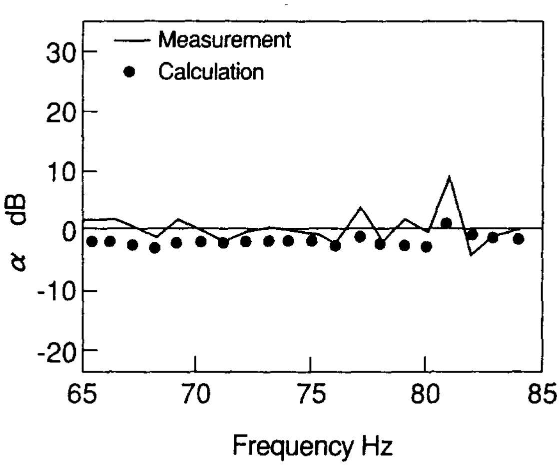

(a) point 3

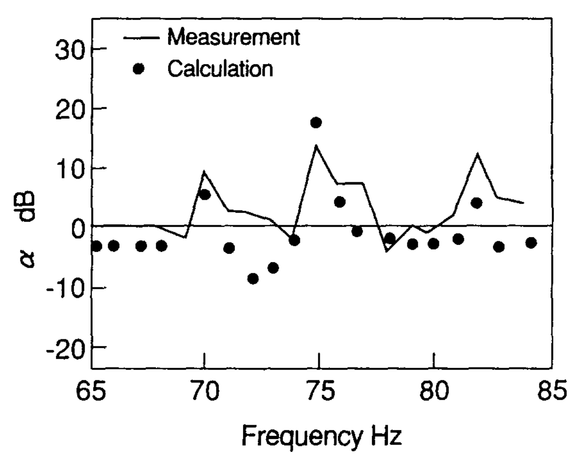

(b) point 25

Fig. 7 Measurement and calculation factor of α

4. Experiment

The experiment for acceleration response was held in a large echoic room. To illustrate the acoustic condition of this room, Figure 8 shows the PSD of SPL at a point in the echoic room with no structure present, and also shows the mean values of 36 points in the echoic room for each 10 Hz frequency band. Usually, in an acoustic test, the condition of SPL is given by the octave band spectram noise, and the acceleration response results are obtained by the PSD. For the calculation of the PSD of acceleration, the force was defined by the distributed SPL of Figure 8. every 1 Hz. Figure 9 shows a comparison of the experimental and the calculated results of the proposed method and the previous method. Figure 10 shows the mean value of Figure 9 every 10 Hz. These results show that the proposed method is more accurate than the previous method.

5. Example for a practical panel

Figure 11 shows an example of the calculation of an acceleration contour map for one panel of a solar array paddle. The designer can determine which points to reinforce by refering to this contour map. Figure 12 shows the frequency responses of acceleration and the stress at points on this panel. The experimental results have no acute peaks, because of the bandwidth of the experimental FFT analysis, but both the amplitude of the experiment and the analysis are of almost the same level.

6. Conclusion

The acoustic loading structure responses at low frequencies were studied, and the following conclusions were made.

(1) A calculation method considering the change of the SPL near the structure and the spatial correlation was derived.

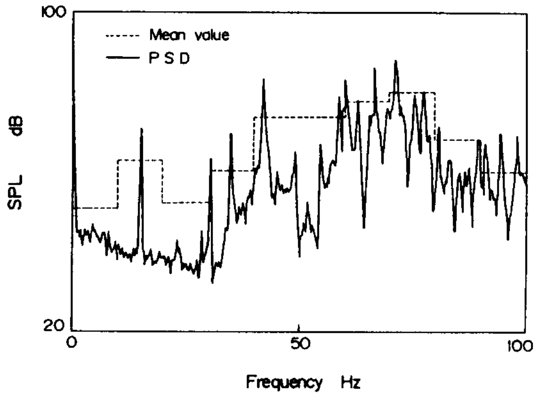

Fig. 8 The SPL without structures

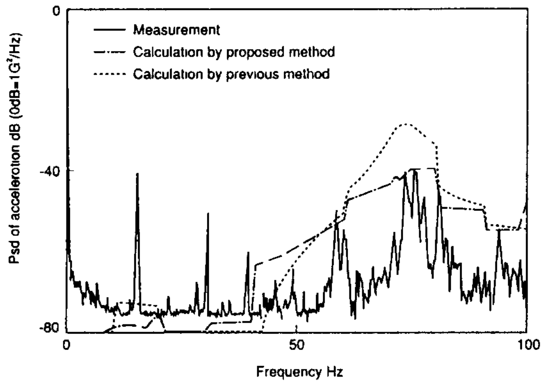

Fig. 9 The PSD of the acceleration (Point 25, bandwidth: 1Hz)

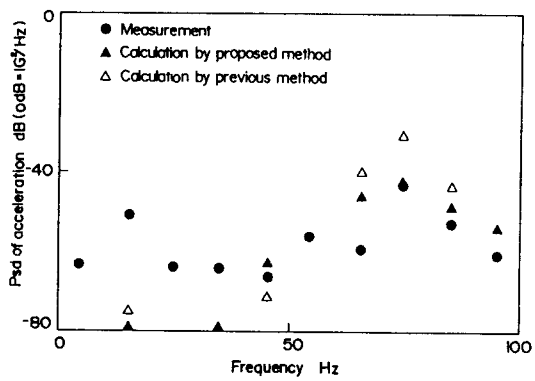

Fig. 10 The PSD of the acceleration (Point 25, bandwidth: 10Hz)

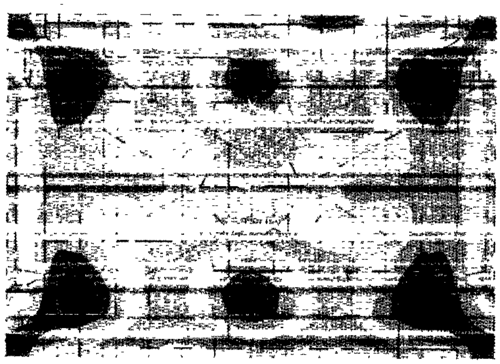

Fig. 11 The contour map of the acceleration of the solar array paddle

(2) The change of SPL near the structure was confirmed by the acoustic test, and the proposed calculation can estimate that change.
(3) The acceleration calculated by the proposed method is more accurate than the previous method.

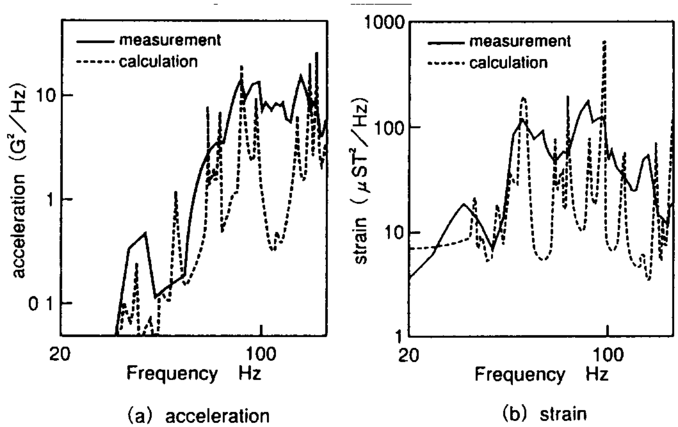

Fig. 12 The PSD of the acceleration and strain of the solar array paddle

References

(1) Yoshida, K., JSME, 58-545, c(1992), 25 (in Japanese).
(2) Yoshida, K., Proceedings of the JSASS/JSME Structures Conference, (1991), 242 (3A7) (in Japanese).
(3) Hayasaka, T., Theory of Sound and Vibration, (1974), 681, Maruzen (in Japanese).
(4) Morrow, C. T., J. Sound Vib., 16-1 (1971), 29-42.
(5) Cook, R. K., J. ASA, 127-6, (1955), 1072-1077.
(6) Chin, C. F., J. Sound Vib., 48-2, (1976), 235-242.
(7) Bendat, J. S., Piersol, A. G., RandomData: Analysis and Measurement Procedures, (1971), John Wiley & Sons Ltd.
(8) Mead, D. J, Noise and Acoustic Fatigue in Aeronautics, (1968), 311, John Wiley & Sons Ltd.
(9) Morse, P., M., Bolt, R., H., Sound Waves in Rooms, Rev. Mos. Phys. No. 2 , (1944).